ISSN 2063-5346

EFFECT OF THE COLLIMATOR DENSITY ON DEPOSITED DOSE IN ORGANS AT RISK ESTIMATED ON A CERVIX PHANTOM USING THE MONTE CARLO SIMULATION PLATFORM GEANT4

Ismail GHAZI[1,*], Mustapha KRIM[2], Othmane KAANOUCH[2,3], El Mehdi ESSAIDI[2], Meriem TANTAOUI[1], and Abdelkrim KARTOUNI[1]

Article History: **Received:** 01.02.2023 **Revised:** 07.03.2023 **Accepted:** 10.04.2023

Abstract

Radiotherapy is a cancer treatment technique that currently occupies an important place in the management of patients. Its challenge is to obtain the best possible compromise between irradiation of the tumor and irradiation of neighboring healthy tissues, which must remain minimal. Optimization of the deposited dose in organs at risk is crucial in radiotherapy treatment. The aim is to emphasize the conformity of lead as a constituent material of the collimator to protect the organs at risk. For this, the demonstration was made on the female pelvic area, which was modeled in the form of a mathematical phantom with real dimensions provided from clinical data, as well as a mobile collimator which makes a rotation of 360° over the phantom, according to the beam axis using the Monte Carlo simulation platform GEANT4. The dose distribution was evaluated based on the values of the Cross-Sections (CS) and Attenuation Coefficients (AC) for photons and electrons, which were calculated using empirical models by the Monte Carlo methods. The dose calculations converge towards the same conclusion with the values of the CS and the AC, which makes it possible to underline the validity and the credibility of the modelization.

Keywords: *Radiotherapy, Collimator, Density, Dosimetry Cervix, Monte Carlo, GEANT4, Cross-Section, Attenuation Coefficient.*

[1]*Subatomic Research and Applications Team, Laboratory of the Physics of Condensed Matter (LPMC-ERSA), Faculty of Sciences Ben M'Sik, Hassan II University, BP 7955, Casablanca, Morocco*

[2]*Hassan First University of Settat, High Institute of Health Sciences, Laboratory of Sciences and Health Technologies, BP 555, 26000, Settat, Morocco*

[3]*Department of Radiotherapy, Sheikh Khalifa International University Hospital, BP 82403, Casablanca, Morocco*

* ***Corresponding author: Ismail GHAZI ;*** *ismailghazi2015@gmail.com,*

DOI: 10.31838/ecb/2023.12.s1.100

1. INTRODUCTION

Morocco recorded a large increase in new cases of cervical cancer between 2012 and 2018, which increased the number of deaths in the Middle East and North Africa region [1]. Cervical cancer ranked as the second leading cause of cancer death in women, not only in Morocco but worldwide. Conversely, in industrialized countries, mortality from cervical cancer has decreased by 50% over the past 40 years, mainly thanks to an effective screening strategy [2].

External radiotherapy has been playing a key role for several decades in the treatment of cancers of the female or male pelvic area [3,4,5] and mainly consists of altering cancer cells using ionizing radiation to cause the death of these harmful cells. Often associated with surgery and chemotherapy, radiotherapy represents a powerful weapon in the resorption of localized tumors. With the constant progress of treatment techniques, the main objective of radiation therapy is to optimize the absorbed dose deposition by maximizing the dose deposited in the tumor while sparing as much as possible the surrounding healthy tissue [6].

However, the present work aims to study the effect of the collimator density on deposited dose in organs at risk estimated on a cervix phantom using the Monte Carlo [7,8,9] simulation platform GEANT4 [10].

This paper is organized as follows. In the second section, we study variation of the cross-section and the attenuation coefficient of photons and electrons for different materials of collimator. In the third section, we present the different methods and materials used in this work. And finally, in the last section, we discuss and interpret the obtained results.

2 CROSS-SECTION AND ATTENUATION COEFFICIENT USING THE MONTE CARLO METHODS

In this part, we study the variation of the cross-section and the attenuation coefficient as a function of the incident energy ranging from 100 eV to 100 MeV for five different materials that we will use later in the composition of the collimator: Aluminum ($Z = 13$; $\rho = 2.699$ g/cm^3) , Iron ($Z = 26$; $\rho = 7.874$ g/cm^3) , Lead ($Z = 82$; $\rho = 11.35$ g/cm^3) , Tungsten ($Z = 74$; $\rho = 19.3$ g/cm^3) and Osmium ($Z = 76$; $\rho = 22.57$ g/cm^3).

The physical processes studied in this work are the photoelectric effect and the Compton scattering effect for photons, and the Bremsstrahlung effect for electrons. These processes will then allow us to evaluate the dose distribution in the organs at risk during the treatment of the cervix in radiotherapy.

2.1 Photons Cross-section and attenuation coefficient

The electromagnetic packages were available in GEANT4 use different empirical and semi-empirical models [11,12]. In this study, we used the Livermore models [13,14] from the Low Energy package. These models include atomic and shell effects, which are typically required for space science, medical physics, and astroparticle applications. The Livermore approach uses evaluated libraries (EPDL97 [15], EEDL [16], and EADL [17]) which provide data for the calculation of the cross-section for photon, electron, and ion interactions with matter.

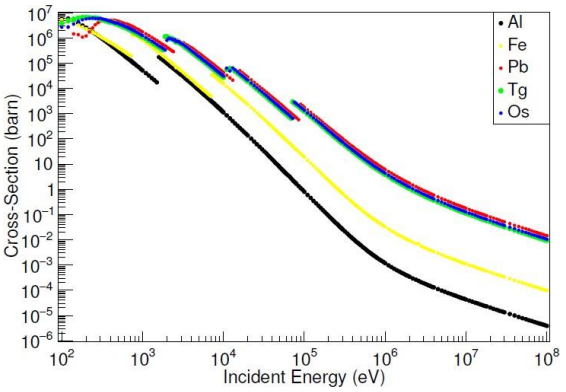

(a) Photoelectric effect CS

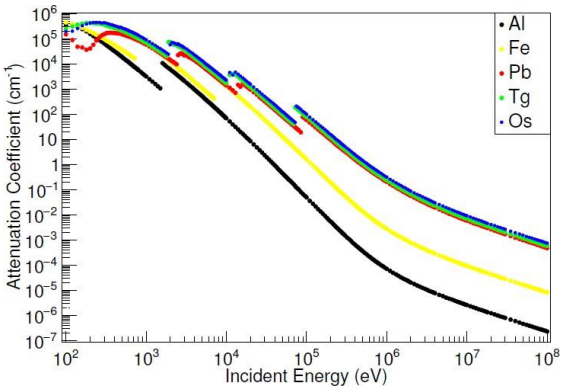

(b) Photoelectric effect AC

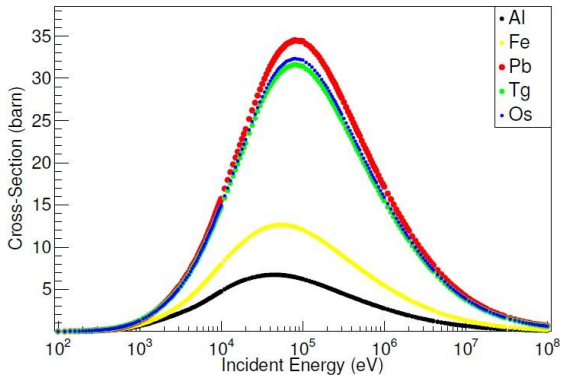

(c) Compton scattering effect CS

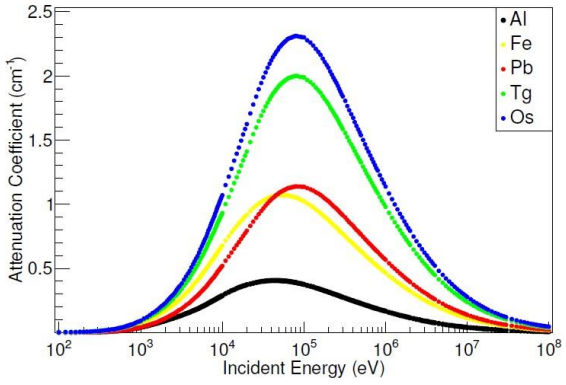

(d) Compton scattering effect AC

Figure 1: Representative curves of the photoelectric effect and Compton scattering effect cross-section (CS) and attenuation coefficient (AC) for different materials.

From the obtained results in Figure 1, we notice that each time the incident energy increases, the variation of the photoelectric cross-section and attenuation coefficient decreases. Hence the appearance of the Compton scattering effect, which is more probable for energies between 1 keV and 10 MeV depending on the density of the material.

The attenuation coefficient, also called the cross-section per volume, was calculated based on the following expression:

$$\mu_l = N_A \frac{\rho}{M} \sigma \qquad (1)$$

With: N_A: Number of Avogadro ; ρ: Density of the material ; M: Molar mass and σ: Cross section per atom.

At low energy, the cross-section (CS) and the attenuation coefficient (AC) of the five materials remain close. But once the incident energy begins to increase, we notice that the variation of the CS and the AC of (Al and Fe) decreases compared to that of (Pb, Tg, and Os) which have remained convergent. This is due to the charge of the nucleus of each atom. The CS and the AC remain important as long as the number of protons in a material is high. On the other hand, the slight difference between the charges of the nuclei of these last three atoms explains the convergence of their CS and AC.

So, for Al and Fe, the photoelectric effect and Compton scattering effect are much weaker than for Pb, Tg, and Os.

Low-energy photons strip away only the least bound and outermost electrons from atoms. This capacity decreases rapidly, until the moment when the energy of the photons exceeds the threshold of the binding energy of the first internal layer of the atom. The photon becomes capable of snatching the electrons deeper from this internal layer [18].

Beyond this threshold, the probability of snatching electrons from the new layer added to that of the previous layers. The probability of the photoelectric effect increases accordingly by making a 'jump'.

The probability of snatching electrons from the new shell decreases in turn until the energy of the photon exceeds the binding energy threshold of electrons in the next shell. As its energy increases, the photon in turn interacts with deeper and deeper layers of the atom [19,20].

Following the emission of the electron, the electronic procession reorganizes by emitting secondary radiation consisting of fluorescence photons (Auger effect).

Lead is much more favorable for radiation protection [21]. It is a very dense material efficient absorber. The binding energies of 3, 20, and 90 keV of the inner shells M, L, and K are much higher. Then the lead core is a heavy core whose property is to promote the photoelectric effect. On the other hand, the property of the tungsten core is to promote the Compton effect.

2.2 Bremsstrahlung Cross-section and attenuation coefficient

In their passage through matter, electrons lose energy in two ways: either by ionization or by braking radiation. The electrons undergo radiative collisions mainly with the atomic nuclei of the medium. In the vicinity of the nucleus, the incident particle undergoes acceleration. According to electrodynamics, a charged particle undergoing acceleration emits radiation. This is called Bremsstrahlung or braking radiation [22,23].

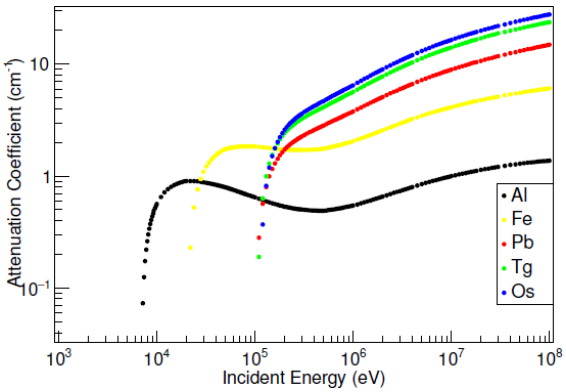

(a) Bremsstrahlung CS

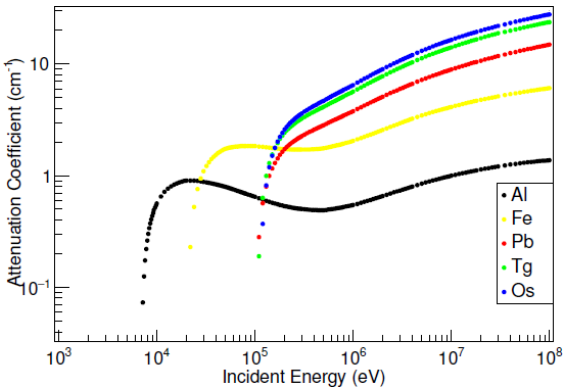

(b) Bremsstrahlung AC

Figure 2: Representative curves of the Bremsstrahlung Cross-section (CS) and attenuation coefficient (AC) for different materials.

From the obtained results in Figure 2, we notice that the variation of the Bremsstrahlung CS and AC of Al and Fe is small compared to Pb, Tg, and Os which remained convergent. This is due to the high load of the nuclei of Pb, Tg and Os compared to Al and Fe.

At low energy, the Bremsstrahlung CS and AC of the five materials are zero because the incident energy of electrons in the order of eV is not sufficient for it to interact with matter.

In addition to the incident energy, the probability of interactions of electrons with matter depends on the density of the material. For low-density materials, the probability of interactions begins for lower energies, and the variation of the CS and AC is always small. The higher the density of the material, the more the probability of interactions will begin for higher energies because low energies cannot penetrate the high-density medium.

So, we can conclude that the interactions of electrons with matter depend on the density of the material as well as the energy of the electron. The more dense the medium is, the more the probability of interactions begins for higher energies.

3 METHODS AND MATERIALS

In this study, we used Monte Carlo method, which is one of the most accurate methods for evaluating the deposited dose in the tumor organ, as well as in organs at risk.

Dose calculations were carried out using GEANT4 Monte Carlo code, version

'10.04.p03'. This code is a software framework for simulating the passage of particles through matter. It is widely used for calculating doses [24,25,26,27,28]. It is the successor to the GEANT software series developed by CERN and the first C++ tool in this field using an object-oriented programming methodology.

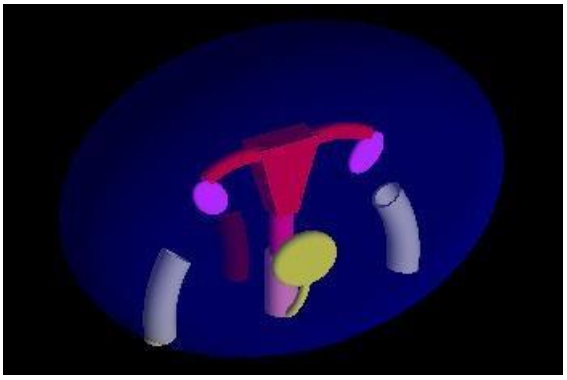

Figure 3: Visualization result of the female pelvic area under GEANT4.

To calculate the deposited dose in the cervix and in the organs at risk, we started by modeling the female pelvic area in the form of a mathematical phantom with real dimensions provided from clinical data. This area is made up of the uterus (body and cervix), bladder, rectum, and the right and left femoral heads which are modeled in a tank as shown in Figure 3.

The tank is represented as an ellipsoid with random dimensions of (10,10,15) cm respectively along (x,y,z). The molecules used in this tank are the water molecules H_2O which are defined in GEANT4 by 'G4_WATER' with a density of 1 g/cm^3.

The body of the uterus is made up of the uterine cavity which is shown as a trapezoid, the right and left fallopian tubes are shown as two tori, and the ovaries as two small ellipsoids. Conversely, the cervix and the vagina are represented in the form of two cylinders with an average length of 3 cm for the cervix and 4 cm for the vagina. The chemical composition used in these geometries is that of blood, which is defined in GEANT4 by 'G4_BLOOD_ICRP' with a density of 1.06 g/cm^3.

The bladder will represent one of the organs at risk. It is schematized in the form of an ellipsoid with real dimensions. The molecules used in this geometry are the water molecules since the bladder is the organ of the urinary system, whose function is to store the terminal urine produced by the kidneys.

The rectum is simplified into a torus. The molecules that we have chosen to represent it are known on GEANT4 under the name 'G4_MUSCLE_STRIATED_ ICRU' with a density of 1.04 g/cm^3, which are composed of a set of eight atoms : (H, C, N, O, Na, P, S and K). Among these atoms, there are six which constitute the components of organic matter (C, H, O, N, P and S).

And finally, the right and left femoral heads are represented as two tori with molecules which are known on GENAT4 as 'G4_BONE_COMPACT_ICRU' with a density of 1.85 g/cm^3.

Then we modeled a collimator which is able to make a rotation of 360° on the phantom according to the direction of the beams of photons, to minimize the deposited dose in the organs at risk. Figure 4 shows the displacement of the collimator at several angles.

The collimator has been simulated using mathematical geometries. It is represented as four blocks. Each block has the following dimension: 20 cm length, 15 cm width, and 3 cm thick. The four blocks of the collimator have been adjusted in a way to conform the tumoral volume and to protect the organs at risk as much as possible. The opening of the window has a square shape with dimensions of 1.5x1.5 cm^2.

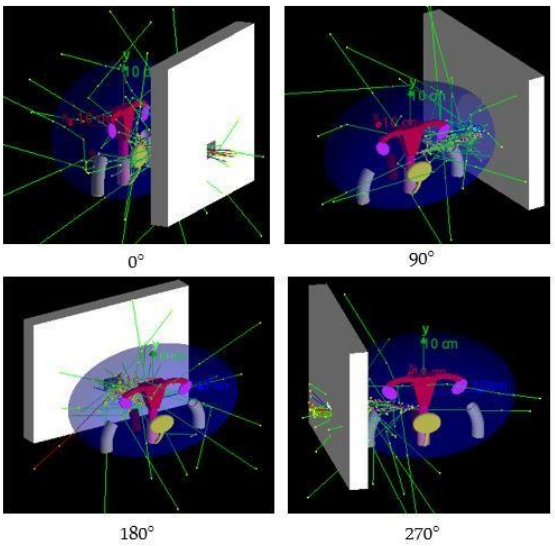

Figure 4: Visualization of collimator by different angles.

The dose is defined as the deposited energy per unit of mass. It is expressed in Gray (Gy).

In GEANT4, the deposited energy E_{dep}, either in the cervix or in the organs at risk is calculated "Step by Step" in the SteppingAction class, then the energy will be accumulated "Event by Event" in the EventAction class. This value is automatically transferred to the RunAction class where GEANT4 calculates the total deposited dose. This calculation is chained by determining the mass of each organ which is calculated from the following expression:

$$m = \rho v \tag{2}$$

Such that ρ is the density of the organ which is declared in the DetectorConstruction class and v its volume.

This then makes it possible to calculate the total deposited dose from the following expression:

$$D_{dep} = \frac{E_{dep}}{\rho v} \tag{3}$$

The photon beams used for irradiation are emitted from a point source with a well-determined direction. The direction of the anterior and posterior beams (0° and 180°) is respectively along the x-axis, with a source-input distance of 20 cm. On the other hand, the lateral beams (90° and 270°) have a direction perpendicular to the x-axis, they are along the z-axis, with a source-input distance of 25 cm, to calculate the dose in the cervix. These photon beams are targeted directly on the tumor organ (cervix) through the collimator window which is open directly on the tumor. This collimator is simulated in a precise way to protect the organs at risk. For this, the opening of the window of the collimator only lets through the photons targeted on the tumor.

4 RESULTS AND DISCUSSIONS

In this section, we investigate the correlation between the deposited dose in the organs at risk and the density of several materials used in the composition of the collimator.

To conduct this study, we have chosen the five materials earlier presented in section 2. Each time we used a material in the collimator, and we irradiated the cervix with beams of photons targeting the beams at the central point of the cervix if we consider that the tumor is in the center, using a direct radioactive source defined in GEANT4, and making a box treatment following four angulations (0°, 90°, 180°, and 270°) to follow the clinical treatment standards, and to have a good dose distribution.

The energy spectrum of 18 MV photons is characterized by average energy of 4.5 MeV and most probable energy of 1.5 MeV [29,30]. For this, we used in our study photon beams with an incident energy of 1.5 MeV and an event number equal to 10^6 photon beams for each angulation. Then we calculated the deposited dose in the cervix and in the organs at risk (bladder, rectum, right femoral head, and left femoral head) to find the optimal material that can attenuate the photon beams scattering and protect the organs at risk as much as possible. The obtained results are shown in Table 1 and Figure 5.

From the obtained results, we notice that the photon beams easily cross low-density materials (Aluminum: $\rho = 2.699$ g/cm^3 and Iron: $\rho = 7.874$ g/cm^3), which produces an important deposited dose in organs at risk, because Al and Fe are both light absorbers where the Compton effect dominates.

When the photon interacts through the Compton effect, it is also absorbed. But alongside the ejected electron, a new photon of lesser energy is emitted. All the kinetic energy carried away by the secondary particles set in motion will not be absorbed locally by the medium. So, the secondary electrons will lose part of their energy by braking radiation. So, to take this fraction of energy lost into account, we consider an energy absorption coefficient.

Table 1: Obtained results for the deposited dose (nGy) in the cervix and in the organs at risk according to the different materials of the collimator.

Collimator materials	Cervix	Bladder	Rectum	Right femoral head	Left femoral head
Aluminum	243.95±4.88	18.11±0.49	3.46±0.10	12.84±0.35	13.45±0.36
Iron	241.17±4.82	16.95±0.46	2.54±0.076	12.03±0.32	11.92±0.32
Lead	244.32±4.88	16.53±0.45	2.14±0.064	11.72±0.32	11.56±0.31
Tungsten	240.04±4.80	17.23±0.47	2.59±0.078	12.65±0.34	12.49±0.34
Osmium	244.13±4.88	17.94±0.48	3.07±0.092	13.48±0.36	13.72±0.37

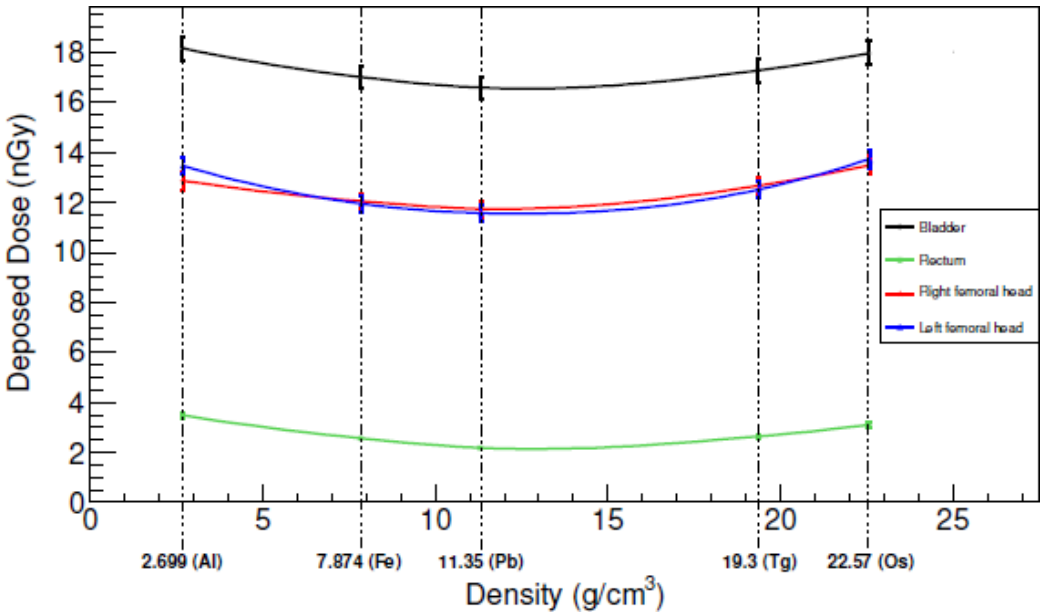

Figure 5: Graphic representation of the deposited dose in the organs at risk according to the different materials of the collimator.

The mass-energy absorption coefficient for uncharged ionizing particles is the product of the mass-energy transfer coefficient by (1-g). Where g the energy fraction of the charged secondary particles which is lost as braking radiation, it is given by the relation:

$$\frac{\mu_{en}}{\rho} = \frac{\mu_{tr}}{\rho}(1-g) \qquad (4)$$

For high-density materials (Tungsten: ρ = 19.3 g/cm^3 and Osmium: ρ = 22.57 g/cm^3), the photons collide for the second time with the Coulomb field of the nucleus of these materials, which makes it possible to reproduce the Bremsstrahlung phenomenon, that is to say, to reproduce by braking radiation photons of higher energy as we saw in the second section. This leads to depositing a large dose in the organs at risk.

Therefore, according to the obtained results, Lead (ρ = 11.35 g/cm^3) is the optimal material that makes it possible to attenuate photons and to protect the organs at risk as much as possible despite the large variation in its cross-section. It is a very efficient absorber. It is first of all a very dense material. Then the lead core is a heavy core whose property is to promote the photoelectric effect.

When the photon interacts by the photoelectric effect, it is absorbed in a single blow by an atom from which it ejects an electron. In the matter of a dense material, the path traveled by this electron is very short, so that we can consider that all its energy is absorbed

locally. For its part, the absorber atom which has lost an electron will reorganize itself and restore the energy acquired by emitting one or more photons. These secondary photons have lost the memory of the direction of the incident photon and are emitted in all directions.

The adjustment of the representative curves of the deposited dose in each organ according to the different material densities was made using the polynomial expression shown in Table 2. These equations represent a modeling of the deposited dose in different organs as a function of the density of the materials.

Table 2: Equations for adjusting the deposited dose in each organ according to the different materials of the collimator.

Organs	**Adjustment equations**
Bladder	$D_d = \alpha\rho^2 + \beta\rho + \gamma$
Rectum	$D_d = \delta\rho^2 + \epsilon\rho + \omega$
Right femoral head	$D_d = \theta\rho^2 + \zeta\rho + \kappa$
Left femoral head	$D_d = \pi\rho^2 + \sigma\rho + \tau$

With: α, β, γ, δ, ϵ, ω, θ, ζ, κ, π, σ and τ represents the adjustment parameters of the representative curves of the deposited dose in each organ as a function of different material densities listed in Table 3.

Table 3: Adjustment parameters of the representative curves of the deposited dose in each organ according to the different densities of the materials.

Organs	**Adjustment parameters**		
Bladder	$\alpha = 19.10\pm0.44$	$\beta = -0.40\pm0.066$	$\gamma = 0.015\pm0.0021$
Rectum	$\delta = 4.34\pm0.45$	$\epsilon = -0.33\pm0.068$	$\omega = 0.012\pm0.0022$
Right femoral head	$\theta = 13.95\pm0.33$	$\zeta = -0.37\pm0.050$	$\kappa = 0.015\pm0.0016$
Left femoral head	$\pi = 14.81\pm0.35$	$\sigma = -0.53\pm0.053$	$\tau = 0.021\pm0.0017$

5 CONCLUSIONS

During the last decades, the use of ionizing radiation in radiotherapy has proven effective in treating cervical tumors.

The main goal of this study was to optimize the deposited dose in the organs at risk by evaluating the collimator density during treatment of the cervix in radiotherapy using the Monte Carlo simulation platform GEANT4.

For this, it was essential to start first with a detailed description of the variation in the cross-section and the attenuation coefficient of photons and electrons for different materials. Then the presentation of the methods and the code used during the simulation, as well as the introduction of some fundamental dosimetric concepts, to properly interpret the obtained results. Using the GEANT4 code, we calculated the deposited dose in the organs at risk of the cervix by using different materials constituting the collimator. We found that Lead (ρ = 11.35 g/cm^3) is the optimal material that allows maximum protection of healthy tissues despite the large variation in its cross-section. Then, we modeled the deposited dose in each organ as a function of the density of materials using second-degree polynomial equations.

REFERENCES

[1] Essaada Belglaiaa and Christiane Mougin. (2019). {Le cancer du col de l'utérus: état des lieux et prévention au Maroc.} Bulletin du Cancer, 6388 (11), 941-1066.

[2] Y. Pointreau, A. Ruffier Loubière, F. Denis and I. Barillot. (2010). {Cancer du col utérin.} Cancer/Radiothérapie, 14, S147-S153.

[3] I. Barillot, C. Haie-Méder, C. Charra Brunaud, K. Peignaux, C. Kerr and L. Thomas (2016). {Radiothérapie des cancers du col et de

l'endomètre.} Cancer/Radiothérapie, 20, S189-S195.

[4] Meriem Tantaoui, Mustapha Krim, Ismail Ghazi, Zineb Sobhy, Abdelkrim Kartouni, Hamid Chakir, Abdenebi El Moutawakkil and Souha Sahraoui (2019). {Dosimetric Comparison of 3D Conformal Radiotherapy (3D-CRT) and Volumetric Modulated Arc Therapy (VMAT®) in Prostate Cancer.} Jour of Adv Research in Dynamical and Control Systems, 11 (11-Special Issue), 653-659.

[5] Meriem Tantaoui, Abdenbi El Moutaoukkil, Mustapha Krim, Ismail Ghazi, Zineb Sobhy, Abdelkrim Kartouni, Hamid Chakir, Jamal Inchaouh, Souha Sahraoui and Hassan Jouhadi (2020). {Statistical Analysis of Dosimetric Data obtained by 3D Conformal Radiotherapy (3D-CRT) and Volumetric Modulated Arc Therapy (VMAT®) in Prostate Cancer.} Jour of Adv Research in Dynamical and Control Systems, 12 (5-Special Issue), 158-167.

[6] R. Mazeron, I. Dumas, C. El Khouri, A. Lévy, M. Attar and C. Haie-Meder (2014). {Radiothérapie conformationnelle avec modulation d'intensité dans les cancers du col : vers un nouveau standard ?} Cancer/Radiothérapie, 18 (2), 154-160.

[7] Arend Matthias G. and Schäfer Thomas (2019). {Statistical power in two-level models: A tutorial based on Monte Carlo simulation.} Psychological Methods, 24 (1), 1-19.

[8] Jian Zhou, Nasim Aghili, Ebrahim Noroozi Ghaleini, Dieu Tien Bui, M. M. Tahir and Mohammadreza Koopialipoor (2020). {A Monte Carlo simulation approach for effective assessment of flyrock based on intelligent system of neural network.} Engineering with Computers, 36, 713-723.

[9] Bill Lozanovski, David Downing, Phuong Tran, Darpan Shidid, Ma Qian, Peter Choong, Milan Brandt and Martin Leary (2020). {A Monte Carlo simulation-based approach to realistic modelling of additively manufactured lattice structures.} Additive Manufacturing, 32, 101092.

[10] Official website of GEANT4. {https://geant4.web.cern.ch/} Accessed: 05 February 2023.

[11] G.A.P. Cirrone, G. Cuttone, F. Di Rosa, L. Pandola, F. Romano and Q. Zhang (2010). {Validation of the Geant4 electromagnetic photon cross-sections for elements and compounds.} Nuclear Instruments and Methods in Physics Research Section A: Accelerators, Spectrometers, Detectors and Associated Equipment, 618 (1), 315-322.

[12] Geant4 Collaboration, Physics Reference Manual, Available Online at. {https://geant4-userdoc.web.cern.ch/UsersGuides/PhysicsReferenceManual/fo/PhysicsReferenceManual.pdf} Accessed: 05 February 2023

[13] Douglass Michael, Bezak Eva and Penfold Scott (2013). {Monte Carlo investigation of the increased radiation deposition due to gold nanoparticles using kilovoltage and megavoltage photons in a 3D randomized cell model.} Medical Physics, 40 (7), 071710.

[14] Liu Ruirui, Zhao Tianyu, Zhao Xiandong and Reynoso Francisco J. (2019). {Modeling gold nanoparticle radiosensitization using a clustering algorithm to quantitate DNA double-strand breaks with mixed-physics Monte Carlo simulation.} Medical Physics, 46 (11), 5314-5325.

[15] Cullen D. E., Hubbell J. H. and Kissel L. (1997). {EPDL97: the evaluated photo data library `97 version.} {https://www.osti.gov/biblio/295438}

[16] Perkins ST, Cullen DE, Seltzer SM and others (1991). {Tables and graphs of electron-interaction cross-sections from 10 eV to 100 GeV derived from the LLNL evaluated electron data library (EEDL), Z= 1-100.} UCRL-50400, 31, 21-24.

[17] Perkins ST, Cullen David, Chen MH, Rathkopf J, Scofield J, and Hubbell JH. (1991). {Tables and graphs of atomic subshell and relaxation data derived from the LLNL Evaluated Atomic Data Library (EADL), Z = 1-100.} UCRL-50400, 30.

[18] Sorokin A. A., Bobashev S. V., Feigl T., Tiedtke K., Wabnitz H. and Richter M. (2007). {Photoelectric Effect at Ultrahigh Intensities.} Phys. Rev. Lett., 99 (21), 213002.

[19] PRATT R. H., RON AKIVA, and TSENG H. K. (1973). {Atomic Photoelectric Effect Above 10 keV.} Rev. Mod. Phys., 45 (2), 273--325.

[20] Adawi I. (1964). {Theory of the Surface Photoelectric Effect for One and Two Photons.} Phys. Rev., 134 (3a), A788--A798.

[21] Patrick Maier, Frederik Wenz and Carsten Herskind (2014). {Radioprotection of normal tissue cells.} Strahlentherapie und Onkologie, 190, 745-752.

[22] Anwar Kamal (2014). {Nuclear Physics.} Springer-Verlag Berlin Heidelberg.

[23] Claude Le Sech and Christian Ngo (2010). {PHYSIQUE NUCLÉAIRE - Des quarks aux applications.} DUNOD.

[24] Othmane Kaanouch, Mustapha Krim, Ismail Ghazi, Kamal Saidi, El Mehdi Essaidi, Meriem Tantaoui and El Madani Saad (2023). {Monte Carlo simulation of the lateral spread for proton beams in voxelized water phantom using GEANT4 platform.} Jpn. J. Appl. Phys. 62, 016005.

[25] Ismail Ghazi, Mustapha Krim, Zineb Sobhy, Meriem Tantaoui, Abdelkrim Kartouni, Hamid Chakir and Jamal Inchaouh (2019). {Measurement and Evaluation of the Deposed Dose by a Beam of Photons in Radiotherapy into the Prostate Using the Monte Carlo Simulation Platform GEANT4.} Jour of Adv Research in Dynamical and Control Systems, 11 (11-Special Issue), 1054-1059.

[26] Ismail Ghazi, Zineb Sobhy, Mustapha Krim, Othmane Kaanouch, Meriem Tantaoui, Abdelkrim Kartouni, Jamal Inchaouh, Hamid Chakir and Said Ouaskit (2021). {Dosimetric Comparison of Radiation Therapy and Proton Therapy in Prostate Cancer Using the Monte Carlo Simulation Platform GEANT4.} Moscow University Physics Bulletin, 76, 326-332.

[27] M. Fiak, A. Fathi, J. Inchaouh, A. Khouaja, A. Benider, M. Krim, N. Harakat, Z. Housni, M. L. Bouhssa, M. Mouadil, Y. Elabssaoui and O. Jdair (2021). {Monte Carlo Simulation of a 18 MV Medical Linac Photon Beam Using GATE/GEANT4.} Moscow University Physics Bulletin, 76, 15-21.}

[28] Chaimaa Elmoujaddidi, Ismail Ghazi, Hamid Chakir, Rajaa Sebihi, Abdelkrim Kartouni and Mustapha Krim (2022). {Monte Carlo GEANT4 Simulation of the Deposited Doses by Different Types of Particles Estimated in a Water Phantom.} Physics of Particles and Nuclei Letters, volume 19, pages 685–692.

[29] George X Ding (2002). {Energy spectra, angular spread, fluence profiles and dose distributions of 6 and 18 MV photon beams: results of monte carlo simulations for a varian 2100EX accelerator.} Phys Med Biol, 47, 1025-1046.

[30] Daryoush Sheikh-Bagheri and D W O Rogers (2002). {Monte Carlo calculation of nine megavoltage photon beam spectra using the BEAM code.} Med Phys, 29, 391-402.